

# Performance Analysis and Impedance Modeling of Rectangular and Circular Split-Ring Resonator Antennas in 2.4/5.2 GHz Bands

Puneet Sehgal<sup>1, 2</sup> and Kamlesh Patel<sup>2, \*</sup>

**Abstract**—In this paper, impedance modeling is presented for analyzing the metallic loading effect on the performance of a split ring resonator (SRR) antenna in (2.4–2.5)/(5.1–5.8) GHz frequency bands. Two SRR antennas of rectangular and circular rings have been designed on ANSYS HFSS software, and their return losses are obtained as  $-16.63/-25.26$  dB at 2.7/5.8 GHz and  $-10/-20.09$  dB at 2.2/5.2 GHz, respectively. Then the metallic loadings are incorporated in both rectangular and circular SRR antennas, which move the peak resonant frequency to 2.5/5.1 GHz with simulated return losses of  $-14.39/-22$  dB for rectangular SRR antenna and to 2.6/5.1 GHz with  $-17.64/-11.10$  dB, respectively for circular SRR antenna. Then, to analyze the effect of metallic loading on SRR antenna performance, a set of equations are derived from the equivalent circuit of the SRR antenna without and with metallic loading to evaluate the lumped elements values. The circular SRR antenna with metallic loading is fabricated, and its measured return loss is found to be  $-17.94/-15.76$  dB at 2.415/5.23 GHz. The lumped component values are calculated from the measured return loss using the derived equations, and these values are compared with those obtained from the simulated return loss for circular SRR antenna. A shift in resonant frequencies towards the desired bands is observed due to the inductive effect of the metallic loading. The axial ratio values higher than 15 dB confirm that the proposed SRR antennas with metallic loadings are linearly polarised. The 2D patterns in  $E$ -plane and  $H$ -plane, as well as 3D far-field patterns, confirm an omnidirectional radiation pattern for circular SRR antenna, which is useful for WLAN applications.

## 1. INTRODUCTION

A pair of C-shaped open loops fabricated on a dielectric substrate is proposed for the realization of negative magnetism, i.e., negative magnetic permeability ( $-\mu$ ), which is commonly known as a split-ring resonator (SRR) [1, 2]. The resonance frequency of the circular SRR (C-SRR) was theoretically determined for edge coupled SRR and broadside coupled SRR [3]. Since then, SRR has found applications in planar microwave filter [4–6], phase shifter [7], power divider [8], leaky-wave antenna [9, 10], etc. So, it is suitable for designing a compact antenna [11]. Thus, a simple structure like SRR in a monopole antenna possesses a resonant property and has been widely explored as a metamaterial, an artificial material that shows the negative values of permittivity and permeability [1, 12, 13]. A dual-band microstrip monopole antenna based on SRR [14] and complementary SRR (CSRR) [15] are proposed which have been reported with an impedance bandwidth (IBW) of 7.5%/25.5% and 31.5%/9.4% at WLAN (2.4/5 GHz) bands, respectively. Such an SRR structure in a monopole antenna reportedly increases the impedance bandwidth and gain in frequency bands of 2.4/5.2 GHz [14–16]. In one of these designs, a concentric split-ring structure with a metallic loading is fed by a coplanar waveguide transmission line and exhibits an impedance bandwidth covering 2.40–2.68 GHz and 3.85–6.95 GHz [16].

---

Received 13 September 2021, Accepted 29 December 2021, Scheduled 2 January 2022

\* Corresponding author: Kamlesh Patel (kpatel@south.du.ac.in).

<sup>1</sup> Atma Ram Sanatan Dharma College, University of Delhi, Dhaula Kuan, New Delhi-110021, India. <sup>2</sup> Department of Electronic Science, University of Delhi South Campus, New Delhi, India.

Also, rectangular split ring resonator (R-SRR) and C-SRR antennas are simulated on an FR4 substrate using ANSYS HFSS software for WLAN applications [17]. In this work, high IBWs of 70.78% in the 5.2 GHz band and 30% in the 2.4 GHz band are achieved for the C-SRR antenna as compared to IBW of 33.84% and 17.90% in the respective bands for the R-SRR antenna in the presence of metallic loadings.

To understand the effect of metallic loading which connects both the rings in such an SRR antenna, its equivalent circuit is presented. Since the modeling of such antennas helps to determine the magnetic resonance frequency (single and multi-band frequencies) along with the impedance matching characteristics, a few models have been proposed earlier for this purpose. The lumped element equivalent circuit models of independent SRR/Complimentary SRR structures and SRR-/Complimentary SRR-loaded lines are reported to obtain their resonance frequency and understand the electromagnetic properties [18, 19]. These models relate the lumped element values to the dimensions of SRR or CSRR. Also, the resonant frequency expressions are simplified to obtain an effective dielectric constant of the substrate with the incorporation of metallic inclusion [20]. However, the analytical expressions discussed in these reports are insufficient to address any physical modification in SRR antenna, like the addition of metallic loading interconnecting two rings or change in the shape of SRR. Therefore, in this paper, an impedance equivalent model is proposed for R-SRR and C-SRR antennas, which models the relationship between the lumped elements values obtained from the simulated or measured return loss characteristics. The methodology presented in this work can be used to study the effect of any metallic inclusion between the rings, and the antenna performance can be optimized to get the desired response for broadband matching and higher gain.

## 2. SRR-BASED ANTENNA DESIGN

The R-SRR and C-SRR monopole antennas fed with a co-planar waveguide (CPW) are designed on an FR4 substrate with substrate parameters  $\epsilon_r$  (dielectric constant) = 4.4,  $h$  (height of substrate) = 1.5 mm, and 35  $\mu\text{m}$  thick copper layer with optimized dimensions as shown in Table 1. In Figures 1(a)–(b),  $L_1$  is the length of the ground plane, and  $L_2$  is the length of the patch whereas  $W_1 = W_3$  is the width of the ground plane, and  $W_2$  is the width of the centered CPW line.  $P_1$  and  $P_2$  are the length and width, respectively for the outer strip in Figure 1(a), whereas  $P_1$  and  $P_2$  are the radii for outer and inner rings with the same center, respectively for the C-SRR antenna in Figure 1(b). In R-SRR and C-SRR antennas, the metallic loadings ( $S_1$  and  $S_2$ ) of 1 mm<sup>2</sup> size connect the two SRR rings [16], and the gap ( $g$ ) in each ring is 1 mm. The C-SRR monopole antenna is fabricated for verification purposes as per the above dimensions and Table 1. Figure 1(c) shows the measurement setup using R&S VNA model ZVH8, and  $S_{11}$  of this antenna is measured after calibration.

**Table 1.** Various dimension parameters of both antenna designs.

| Various parameters      | R-SRR antenna | C-SRR antenna |
|-------------------------|---------------|---------------|
| $L_1$ (mm)              | 40            | 43            |
| $L_2$ (mm)              | 22            | 22            |
| $W_1 = W_3$ (mm)        | 11            | 11            |
| $W_2$ (mm)              | 3             | 3             |
| $P_1$ (mm)              | 20            | 7.5           |
| $P_2$ (mm)              | 13            | 5.5           |
| Size (mm <sup>3</sup> ) | 40 × 26 × 1.5 | 43 × 26 × 1.5 |

The simulated return loss ( $S_{11}$ ) responses of R-SRR without and with metallic loadings along with simulated  $S_{11}$  C-SRR without and with metallic loadings and measured  $S_{11}$  response are shown in Figure 2(a). R-SRR antenna without metallic loadings exhibits simulated  $S_{11}$  of minimum  $-16.63/-25.26$  dB at 2.7/5.8 GHz and  $-17.64/-11.10$  dB with metallic loadings at 2.6/5.1 GHz, respectively; however, at 2.4/5.2 GHz, the  $S_{11}$  values are  $-23.78/-15.24$  dB. The new design C-SRR

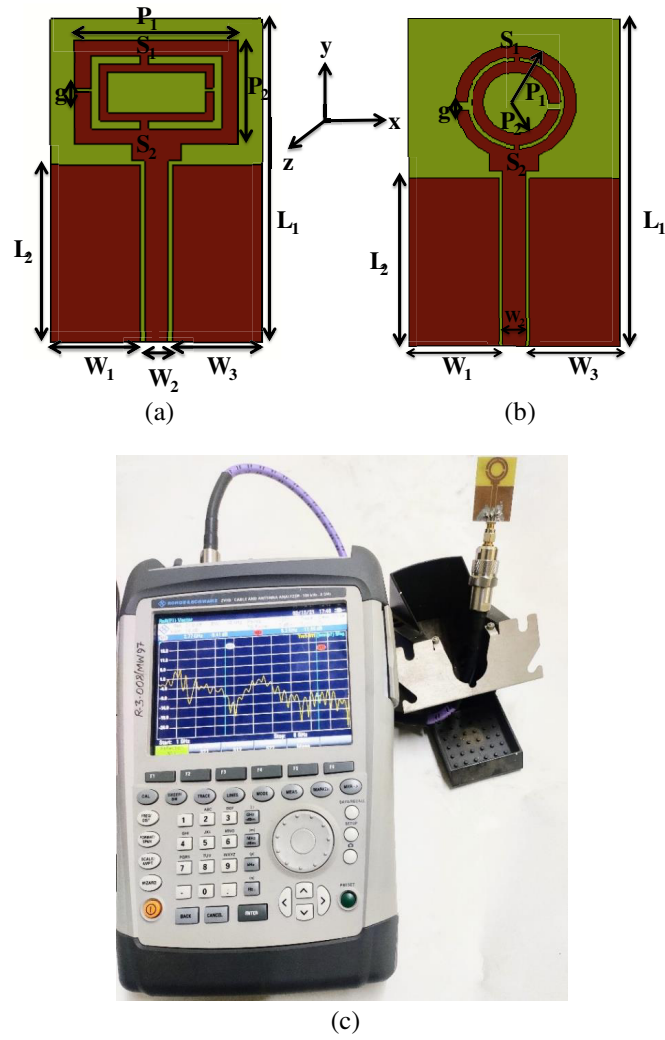


**Figure 1.** Design of (a) the rectangular SRR antenna, (b) the circular SRR antenna, (c) measurement setup with R&S VNA.

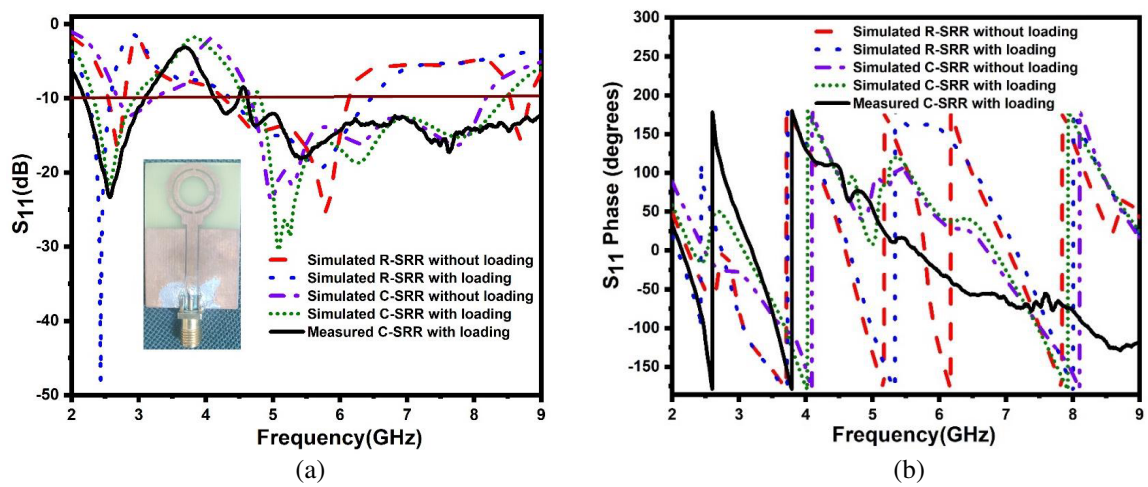


**Figure 2.** (a) Return loss characteristics. (b) Return loss (phase) characteristics.

antenna without metallic loadings exhibits simulated minimum  $S_{11}$  of  $-10/-20.09$  dB at 2.2/5.2 GHz and  $-14.39/-22$  dB in the presence of metallic loadings at 2.5/5.1 GHz. The same antenna with metallic loading gives  $S_{11}$  of  $-13.03/-26.47$  dB at 2.4/5.2 GHz, while measured  $S_{11}$  of C-SRR antenna with metallic loadings is obtained as  $-17.94/-15.76$  dB at 2.415/5.23 GHz frequency. From Figure 2(b), it can be observed that the simulated phase of  $S_{11}$  (in degrees) at 2.7/5.1 GHz is  $-26.84^\circ/-16.55^\circ$  for R-SRR antenna without metallic loadings and  $44.72^\circ/-129.22^\circ$  at 2.6/5.1 GHz for R-SRR antenna with metallic loadings, respectively, whereas for C-SRR antenna without metallic loadings, the simulated phase is  $51.19^\circ/83.14^\circ$  at 2.2/5.2 GHz and  $-16.07^\circ/122.4^\circ$  for C-SRR antenna with metallic loadings at 2.5/5.1 GHz, respectively. The phase of  $S_{11}$  for C-SRR antenna with metallic loadings is measured as  $-76.63^\circ/17.47^\circ$  at 2.415/5.23 GHz. Thus, the phase deviation of  $430.41\%/ -79.08\%$  is observed at 2.415/5.23 GHz, respectively, to the simulated phase values, which confirms the large phase shift between the measured and simulated results of C-SRR antenna while keeping the same pattern of phase variation with frequency as in Figure 2(b).

### 3. MODELING OF ANTENNA DESIGNS

#### 3.1. Modeling of Circular SRR Antenna

An equivalent circuit model of the C-SRR antenna of Figure 1(b) is shown in Figure 3. When a magnetic field is applied along say  $z$ -axis, an electromotive force (e.m.f) develops around the SRR ring structure and is responsible for coupling between the rings. Hence, a continuous current is passing from one ring to another [18, 19], which induces an inductance ( $L$ ) as shown in Figure 3. Due to spacing  $d$  ( $= 0.5$  mm) between the rings, the distributed capacitances ( $C_1, C_2$ ) are formed at the two halves of the SRR structure above and below the split gaps whereas the gap capacitances ( $C_{g1}, C_{g2}$ ) are formed due to split within the inner and outer rings [18–20]. Thus, it acts as an L-C tank circuit that operates at a particular resonance frequency for a single ring of SRR [19, 20]. For a wire loop of the rectangular cross-section with a length  $L$  (in mm) and thickness  $t$  ( $= 1.5$  mm), the equivalent inductance  $L$  is given by [18]

$$L = 0.0002l \left( 2.303 \log_{10} \frac{4l}{t} - \emptyset \right) \mu\text{H} \quad (1)$$

In the above Equation (1),  $\emptyset = 2.451$  is a constant for a wire loop of circular geometry, and the length  $l$  can be expressed as  $l = 6P_1 - g$ . Here, length  $l$  is estimated by considering a single loop with an outer radius  $P_1$  of the C-SRR ring (Figure 1(b)), and the mutual inductance between the rings has been ignored [18].

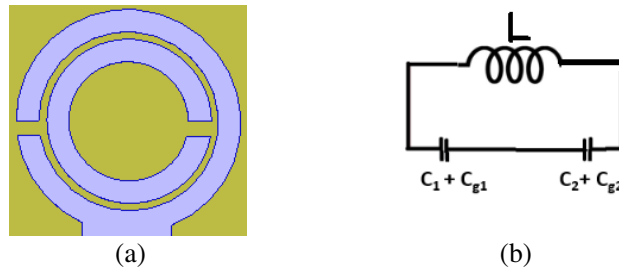


**Figure 3.** (a) Circular SRR structure. (b) Equivalent circuit model of circular SRR antenna.

The equivalent circuit of C-SRR structure of Figure 3(a) is shown in Figure 3(b), so the net capacitance ( $C$ ) of this equivalent circuit can be expressed in terms of capacitances [18],

$$C = \frac{(C_1 + C_{g1})(C_2 + C_{g2})}{(C_1 + C_{g1}) + (C_2 + C_{g2})} \quad (2)$$

where  $C_{g1}$  and  $C_{g2}$  are the gap capacitances (since  $g_1 = g_2 = g$ ), and series distributed capacitance  $C_1$  and  $C_2$  are of the same magnitude.

After subsequent steps given in [18], the net capacitance of the SRR ring is

$$C = \frac{(3P_{avg} - g) C_{pul}}{2} + \frac{\varepsilon_0 t d}{2g} \quad (3)$$

where  $P_{avg}$  = average dimension of the ring,  $g$  = gap in rings, and  $C_{pul}$  = capacitance per unit length along the ring dimensions. Thus, a resonant frequency ( $f_r = \frac{1}{2\pi\sqrt{LC}}$ ) can be represented in terms of physical dimensions of the SRR as follows [18]

$$f_r = \frac{1}{2\pi\sqrt{0.0002l(2.303 \log_{10} \frac{4l}{t} - \emptyset) \left[ \frac{(3P_{avg} - g) C_{pul}}{2} + \frac{\varepsilon_0 t d}{2g} \right]}} \quad (4)$$

Using the above expressions, the resonance frequencies of outer and inner rings are estimated from the physical dimensions of optimized C-SRR and are given in Table 2.

**Table 2.** The calculated resonance frequency and physical dimensions of a C-SRR antenna.

| Various parameters                  | Outer ring | Inner ring |
|-------------------------------------|------------|------------|
| $t$ (mm)                            | 1.5        | 1.5        |
| $d$ (mm)                            | 0.5        | 0.5        |
| $C$ (fF)                            | 200.23     | 127.319    |
| $l$ (mm)                            | 44         | 32         |
| $g$ (mm)                            | 1          | 1          |
| $L$ ( $\mu$ H)                      | 0.0204     | 0.01277    |
| $f_r$ (GHz) — calculated            | 2.5        | $\sim 4$   |
| $f_r$ (GHz) — targeted (simulation) | 2.4        | 5.2        |

Thus, for the C-SRR antenna, the calculated resonant frequencies obtained from the above modeling equations are in close approximation for low resonant frequencies, i.e., 2.5 GHz and 2.4 GHz, while the difference is large for high resonant frequencies, i.e., between 4 GHz and 5.2 GHz. This larger difference in high resonant frequency estimation for the inner ring is due to two reasons: first, in the simulation, the outer ring is excited which in turn induces the magnetic flux in the inner ring although the metallic loadings are placed so that more current flows into the inner ring at the higher frequency. Secondly, as the mutual coupling develops between two rings in the simulation, the total inductance at high frequency is decreased due to two parallel opposing rings compared to a single ring that has zero mutual inductance. This led to achieving the targeted frequency in simulation. In this case, computation of indirectly excited ring inductance and accurate estimation of the resonant frequency require further in-depth analysis.

### 3.2. Proposed Impedance Modeling of Rectangular and Circular SRR Shaped Antenna

In the analytical modeling discussed in Section 3.1, the values of lumped element and resonant frequency can deviate at the higher frequency from the target values. In addition, the above equations become invalid for the case of any modifications made in such an SRR antenna. Modifications are required in SRR antennas to either enhance impedance bandwidth or gain. A technique of modeling is required to analyze the effect of any modifications made in the SRR antenna. The input impedance  $Z_{in}$  (or admittance  $Y_{in}$ ) value is obtained from the complex reflection coefficients or  $S_{11}$  data as  $Z_{in} = Z_0[(1+S_{11})/(1-S_{11})]$ . The values of input impedance and admittance of both R-SRR and C-SRR antennas are shown in Table 2, which are obtained from simulated and measured  $S_{11}$  values (Figure 2).

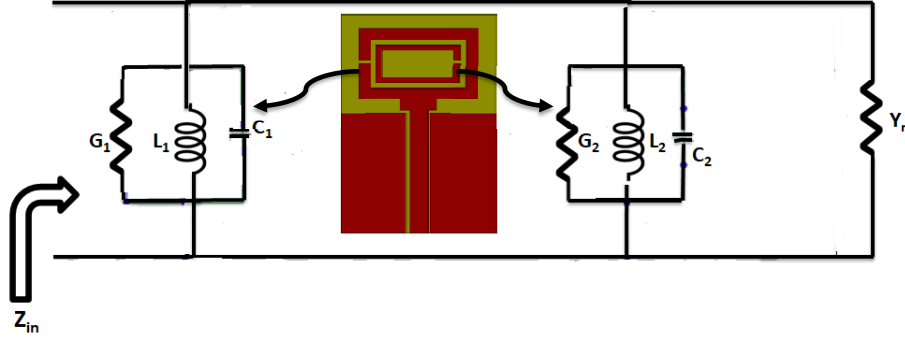


**Figure 4.** Equivalent impedance circuit of the rectangular SRR antenna without metallic loading.

Figure 4 presents the equivalent circuit of the R-SRR antenna without metallic loading, which is used to calculate the impedance of the circuit, and hence the values of lumped elements ( $L_1$ ,  $L_2$ ,  $C_1$ ,  $C_2$ ) can then be obtained. So, the equivalent admittances  $Y_1$  and  $Y_2$  are represented as,

$$Y_1 = G_1 + \frac{1}{j\omega L_1} + j\omega C_1 \quad (5)$$

$$Y_2 = G_2 + \frac{1}{j\omega L_2} + j\omega C_2 \quad (6)$$

Here,  $Y_1$  and  $Y_2$  are the individual combination of ( $L_1, C_1, G_1$ ) and ( $L_2, C_2, G_2$ ), respectively for the outer ring with length  $P_1$  and the inner ring with width  $P_2$  of the SRR antenna.

Hence, the net equivalent input admittance of the circuit  $Y_{in}(= \frac{1}{Z_{in}})$  in Figure 4 is,

$$Y_{in} = Y_1 + Y_2 + Y_n \quad (7)$$

$$Y_{in} = G_1 + G_2 + \frac{1 - \omega^2 L_1 C_1}{j\omega L_1} + \frac{1 - \omega^2 L_2 C_2}{j\omega L_2} + Y_n \quad (8)$$

where  $Y_n = \frac{1}{Z_n} = 0.003 \frac{\text{mho}}{\text{m}}$  is the intrinsic admittance of the free space.

Since the R-SRR antenna without metallic loading resonates at two frequencies, 2.7 GHz and 5.8 GHz, respectively, as mentioned in Table 3, the values of lumped elements ( $L_1, C_1, G_1$ ) and ( $L_2, C_2, G_2$ ) can be obtained from the simulated  $S_{11}$  values of SRR antennas. So, at  $f_{01}$  (first resonant frequency) = 2.7 GHz corresponding to  $\omega_{01} = 16.956 \times 10^9$  rad/s and at  $f_{02}$  (second resonant frequency) = 5.8 GHz corresponding to  $\omega_{02} = 36.42 \times 10^9$  rad/s, the following equations are related with the lumped element values,

$$\omega_{01} = \frac{1}{\sqrt{L_1 C_1}} \quad \text{And} \quad \omega_{02} = \frac{1}{\sqrt{L_2 C_2}} \quad (9)$$

From Equations (5) to (9), the lumped elements values are calculated as,  $L_1 = 285.18 \mu\text{H}$  and  $C_1 = 0.012 \text{fF}$  at 2.7 GHz and  $L_2 = 602.4 \text{nH}$  and  $C_2 = 1.25 \text{fF}$  at 5.8 GHz. In general, a negative inductance can be seen as a capacitor at a fixed frequency, which gives the same reactance as an inductor but with the opposite phase. Hence, in our case, the antenna portion modeled as the inductor produces the capacitance at the frequencies under consideration and vice versa. The equivalent circuit for the R-SRR antenna with metallic loading (Figure 1(a)) is shown in Figure 5. Here, the series combination of conductance  $G_3$  and inductance  $L_3$  is introduced by considering the inductive effect of metallic loading which results in the slight shifting of resonant frequencies to 2.6/5.1 GHz, respectively. From simulation data, the values of input impedance and admittance at 2.6/5.1 GHz are shown in Table 3 for the R-SRR antenna with metallic loadings.

Using the equivalent model of Figure 5, the net input admittance of the circuit can be expressed as

$$Y_{in} = Y_{11} - \frac{(Y_{21} Y_{12})}{Y_{22}} \quad (10)$$

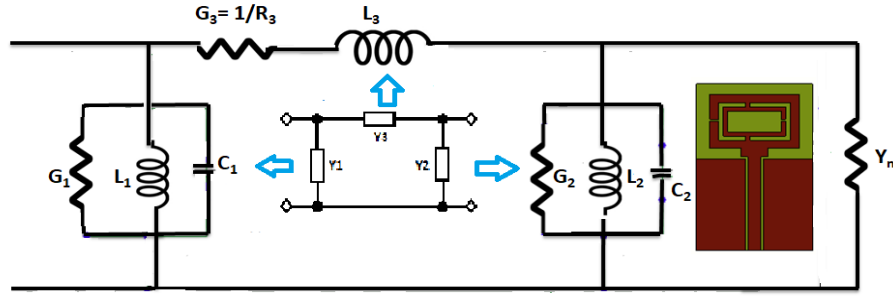


Figure 5. Equivalent impedance circuit of the rectangular SRR antenna with metallic loading.

Table 3. Impedance and admittance values of the C-SRR antenna.

| Antenna type                           | Frequency (GHz)  | $Z_{in}$ ( $\Omega$ ) | $Y_{in}$ (mhos or S) |
|--|------------------|-----------------------|----------------------|
| R-SRR antenna without metallic loading | 2.7 (simulated)  | $48.26 - j9.22$       | $0.02 + j0.004$      |
|  | 5.8 (simulated)  | $45.98 + j0.034$      | $0.022 - j0$         |
| R-SRR antenna with metallic loading    | 2.6 (simulated)  | $55.34 - j7.60$       | $0.018 - j0.002$     |
|  | 5.1 (simulated)  | $29.57 + j4.78$       | $0.033 + j0.005$     |
| C-SRR antenna without metallic loading | 2.2 (simulated)  | $28.83 + j92.03$      | $0.003 - j0.01$      |
|  | 5.2 (simulated)  | $48.35 + j9.91$       | $0.02 - j0.004$      |
| C-SRR antenna with metallic loading    | 2.5 (simulated)  | $58.32 - j2.49$       | $0.017 + j0.001$     |
|  | 5.1 (simulated)  | $48.28 + j3.75$       | $0.021 - j0.002$     |
|  | 2.415 (measured) | $52.734 - j12.83$     | $0.0179 + j0.0044$   |
|  | 5.23 (measured)  | $50.5197 - j16.59$    | $0.0179 + j0.0059$   |

where,  $Y_{11} = Y_1 + Y_3$ ,  $Y_{22} = Y_2 + Y_3$ ,  $Y_{21} = Y_{12} = -Y_3$ , thus

$$Y_{in} = (Y_1 + Y_3) - \frac{(Y_3^2)}{(Y_2 + Y_3)} \tag{11}$$

here  $Y_3 = G_3 + \frac{1}{j\omega L_3}$ . So, Equation (11) becomes

$$Y_{in} = G_1G_2 + G_1G_3 + G_3G_2 + \frac{(1 - \omega^2L_2C_2)}{j\omega L_2} (G_1 + G_3) + \frac{(1 - \omega^2L_1C_1)}{j\omega L_1} (G_2 + G_3) - \left[ \frac{(1 - \omega^2L_1C_1)}{\omega^2L_1L_3} + \frac{(1 - \omega^2L_2C_2)}{\omega^2L_1L_2} \right] - \left[ \frac{(1 - \omega^2L_1C_1)(1 - \omega^2L_2C_2)}{\omega^2L_1L_2} \right] \tag{12}$$

Since  $Y_{in} = G_{in} + jB_{in}$  where  $G_{in}$  is the input conductance and  $B_{in}$  the input susceptance, comparing the real and imaginary parts, we get

$$G_{in} = G_1G_2 + G_1G_3 + G_3G_2 - \left[ \frac{(1 - \omega^2L_1C_1)}{\omega^2L_1L_3} + \frac{(1 - \omega^2L_2C_2)}{\omega^2L_1L_2} \right] - \left[ \frac{(1 - \omega^2L_1C_1)(1 - \omega^2L_2C_2)}{\omega^2L_1L_2} \right] \tag{13}$$

$$B_{in} = \frac{(1 - \omega^2L_2C_2)}{j\omega L_2} (G_1 + G_3) + \frac{(1 - \omega^2L_1C_1)}{j\omega L_1} (G_2 + G_3) \tag{14}$$

Using Equations (13)–(14), the lumped element values are calculated as  $L_3 = 249.74$  fH and  $G_3 = 337.43$  S for the R-SRR antenna to represent the effect of metallic loading. Thus, the values of lumped elements can be realized from its equivalent impedance model for any SRR antenna. In the same way, the lumped elements values are obtained for the C-SRR antenna without metallic loading resonating

at 2.2/5.2 GHz and with metallic loading resonating at 2.5/5.1 GHz. These lumped elements values are obtained as  $L_1 = 343.812$  nH and  $C_1 = 0.1524$  fF at 2.5 GHz and  $L_2 = 6.00241$  nH and  $C_2 = 0.1562$   $\mu$ F at 5.1 GHz using Equations (8)–(14). For the C-SRR antenna with metallic loading,  $L_3 = 0.15$  nH and  $G_3 = 42.46$  S are obtained. From measured  $S_{11}$  of the fabricated C-SRR antenna, it was observed that it resonates at  $f_{01}$  (first resonant frequency) = 2.415 GHz corresponding to  $\omega_{01} = 15.166 \times 10^9$  rad/s and at  $f_{02}$  (second resonant frequency) = 5.23 GHz corresponding to  $\omega_{02} = 32.844 \times 10^9$  rad/s. Thus, using the same Equations (8)–(14), the lumped parameters are obtained as  $L_1 = 19.14$  nH and  $C_1 = 0.227$  pf,  $L_2 = 11.791$  nH and  $C_2 = 78.63$  fF,  $L_3 = 3.08$  nH, and  $G_3 = 0.99$  S. Between the simulated and measured  $S_{11}$  for C-SRR antenna, the resonant frequency is found to be shifted a little due to fabrication tolerances, so the different values of lumped components are obtained.

Since the values of lumped components in modeling of C-SRR antenna are different using the simulated and measured  $S_{11}$ , the simulated input conductance and susceptance of R-SRR and C-SRR antennas with metallic loadings as well as the measured input conductance and susceptance of C-SRR antenna with metallic loadings are studied with frequency as shown in Figures 6(a)–(b). The values of simulated conductance for R-SRR and C-SRR antennas are obtained as 13.63/32.05 mS at 2.6/5.1 GHz and 18.41/20.59 mS at 2.5/5.1 GHz respectively while the measured conductance for C-SRR antenna is 1790/17.87 mS at 2.415/5.23 GHz. For the R-SRR antenna, the peak conductance values are obtained as 62.67 mS at 3.7 GHz and 79.85 mS at 8 GHz; otherwise, the values are less than 50 mS whereas a single high peak value is observed as 147.73 mS at 4 GHz with simulated results and 78.26 mS at 3.815 GHz from the measured values for C-SRR antenna. Since the skin depth varies as the inverse of  $\sqrt{f}$ , the conductance slightly changes with frequency [21]. Also, with the change in shape from rectangle to circle, the dimension changes are governed by the relation  $\frac{R_{ac}}{R_{dc}} = \frac{a}{2} \sqrt{\pi f \mu \sigma}$  [21], where  $a$  is the radius of the conductor wire or dimensional parameter for any shape.

Similarly in the susceptance ( $B_{in}$ ) plot as shown in Figure 6(b), the capacitance changes to inductance at these switch over frequencies for SRR antennas. The susceptance is found to be  $-7.63/6.55$  mS at 2.6/5.1 GHz for R-SRR antenna, and in C-SRR antenna, it is found to be 0.73/ $-1.6$  mS at 2.5/5.1 GHz from simulated values and 4.36/5.87 mS at 2.415/5.23 GHz from the measured value, as the inductance of SRR antenna increases, its susceptance becomes more negative.

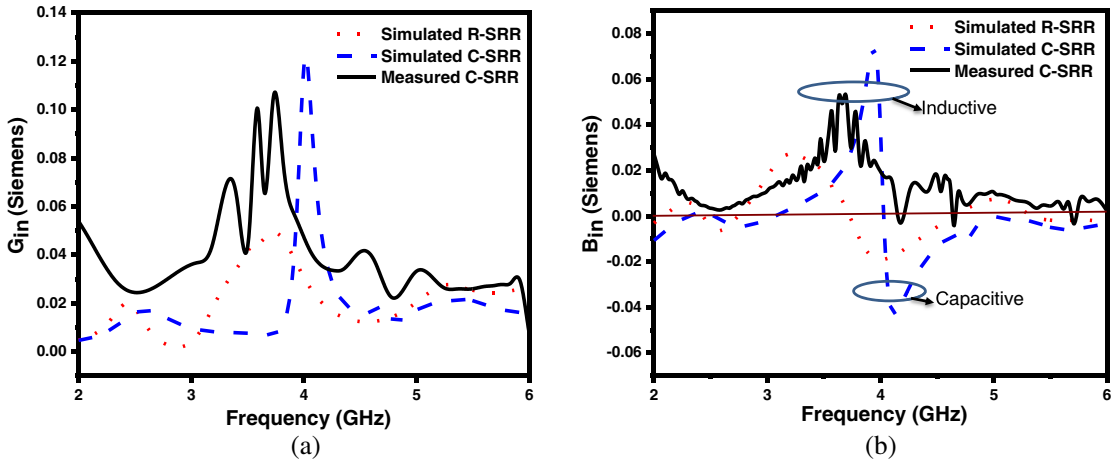


**Figure 6.** (a) Conductance response of the antenna. (b) Susceptance plot.

#### 4. ANTENNA PARAMETERS RESULTS

Figure 7(a) presents the peak directivity (in dB) of the proposed SRR antennas along with the frequency range. It is found that with increasing frequency, a maximum peak directivity value of 4.13 dB is obtained at 5.1 GHz for C-SRR antenna with metallic loading, which is 2.23% greater in the peak directivity in comparison to C-SRR antenna without metallic loading. In the same band, the maximum

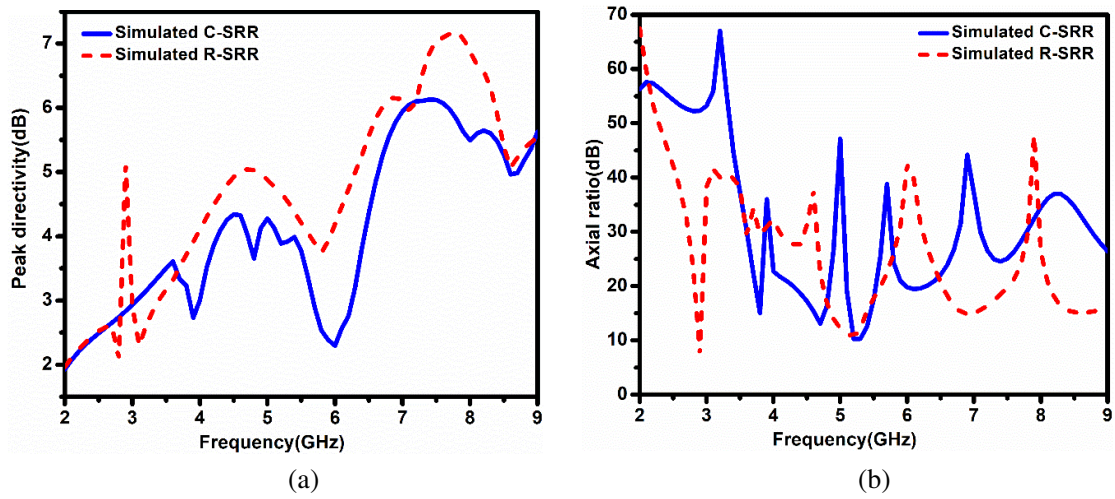


Figure 7. (a) Peak directivity of the antenna. (b) Axial ratio of the antenna.

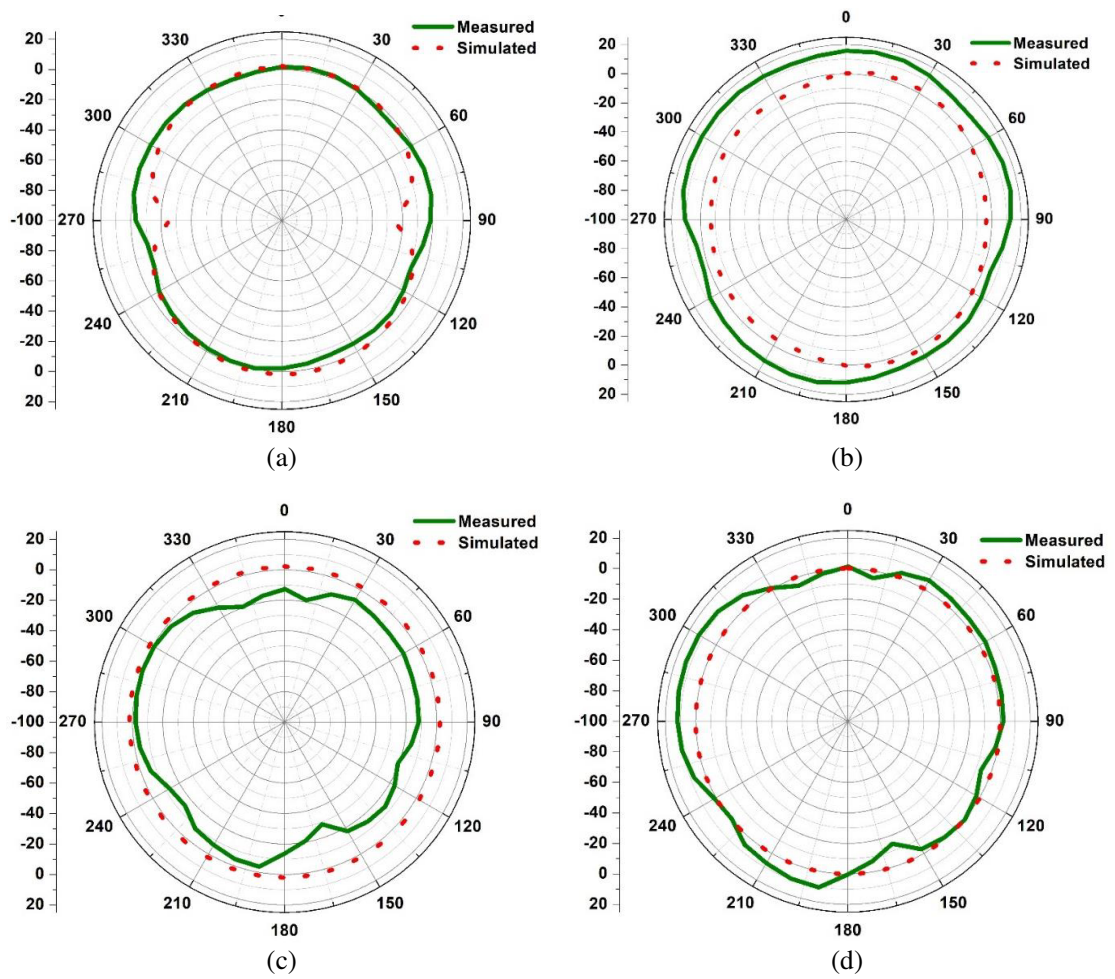


Figure 8. 2-D radiation patterns with (a) *E*-plane at 2.4 GHz, (b) *E*-plane at 5.2 GHz, (c) *H*-plane at 2.4 GHz, (d) *H*-plane at 5.2 GHz.

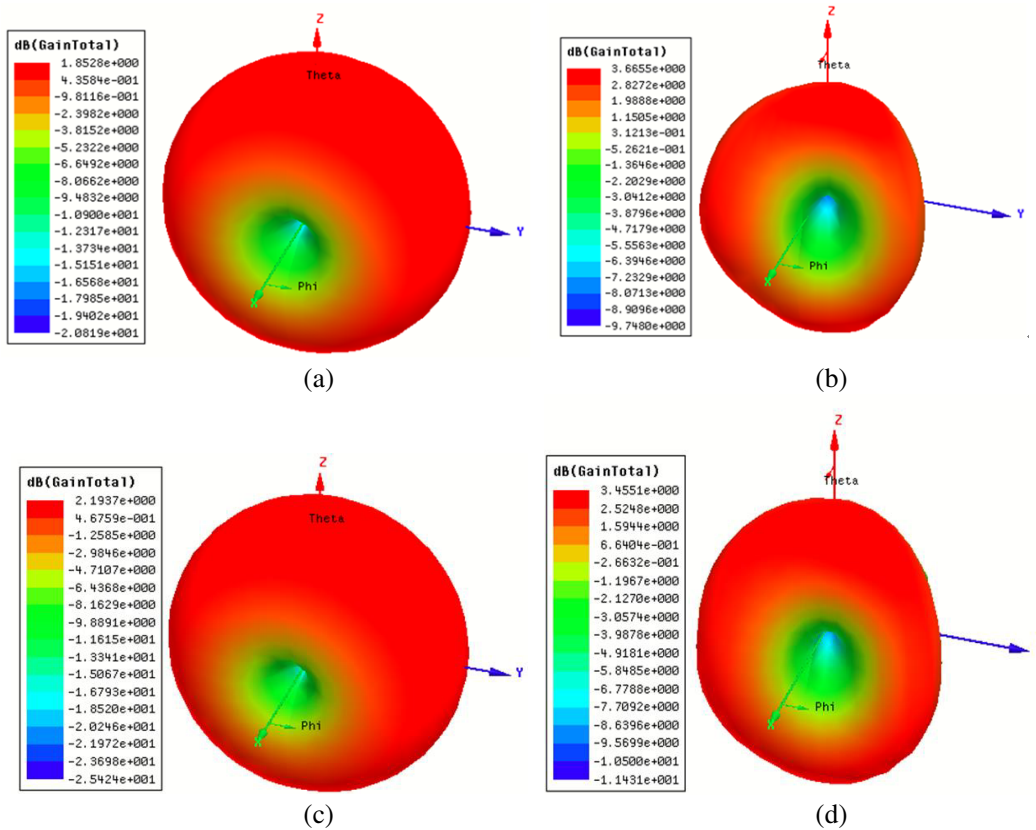
**Table 4.** AR and directivity values of the R-SRR and C-SRR antenna with metallic loadings.

| Frequency (GHz) | AR value (dB)       | Directivity value (dB) |
|-----------------|---------------------|------------------------|
| 2.2–3.0         | 53.32–38.28 (R-SRR) | 2.24–2.92 (R-SRR)      |
|                 | 57.35–53.18 (C-SRR) | 2.2–2.93 (C-SRR)       |
| 4.4–9.0         | 27.69–16 (R-SRR)    | 4.8–5.56 (R-SRR)       |
|                 | 18.72–27.4 (C-SRR)  | 4.26–5.63 (C-SRR)      |

peak directivity is 4.88 dB for the R-SRR antenna with metallic loading. Similarly, in the 2.4 GHz band, it is 2.6 dB for both R-SRR antenna and C-SRR antennas with metallic loading.

An axial ratio (AR) plot shown in Figure 7(b) represents the linear polarization in these antennas in respect to frequency with fluctuations in AR values as these values are higher than 15 dB in the large frequency range. The AR and directivity values in the given range are summarized in Table 4 for both antennas.

Figures 8(a)–(b) show the 2-D radiation patterns in the  $E$ -plane ( $\theta$  is variable and  $\varphi = 0^\circ$ ) at 2.4 GHz and 5.2 GHz, respectively, whereas Figures 8(c)–(d) show in  $H$ -plane ( $\varphi$  is variable and  $\theta = 90^\circ$ ) at 2.4 GHz and 5.2 GHz, respectively. In both the planes, the C-SRR antenna radiates an omnidirectional pattern, and also, the measured results closely resemble simulated ones. 3-D far-field patterns are shown in Figure 9 only for the C-SRR antenna to understand its directional properties concerning the metallic loading. In comparison, the C-SRR antennas are found to be more directional with the metallic loading.

**Figure 9.** 3-D far-field patterns of the C-SRR antenna without metallic loading (a) at 2.4 GHz, (b) at 5.2 GHz, and C-SRR antenna with metallic loading (c) at 2.4 GHz, (d) at 5.2 GHz.

The C-SRR antenna without the metallic loading shows the again of 1.85 dB at 2.4 GHz and 3.67 dB at 5.2 GHz, respectively, while the metallic loading improves the gain to 2.1 dB at 2.4 GHz, and a similar gain of 3.46 dB is observed at 5.2 GHz, as in Figure 9.

The surface current distribution of the C-SRR antenna is shown in Figure 10 which confirms that in the SRR antenna without metallic loading, the radiation occurs only from one ring at the corresponding resonating frequency, i.e., 2.4 GHz for the outer ring and 5.2 GHz for the inner ring. In Figures 10(a)–(b), the surface current density is in the range of about 3.91 to 11.5 A/m for the outer ring of C-SRR antenna without metallic loading at 2.4 GHz while it is about 7.15 to 21.1 A/m for inner ring resonating at 5.2 GHz, respectively.

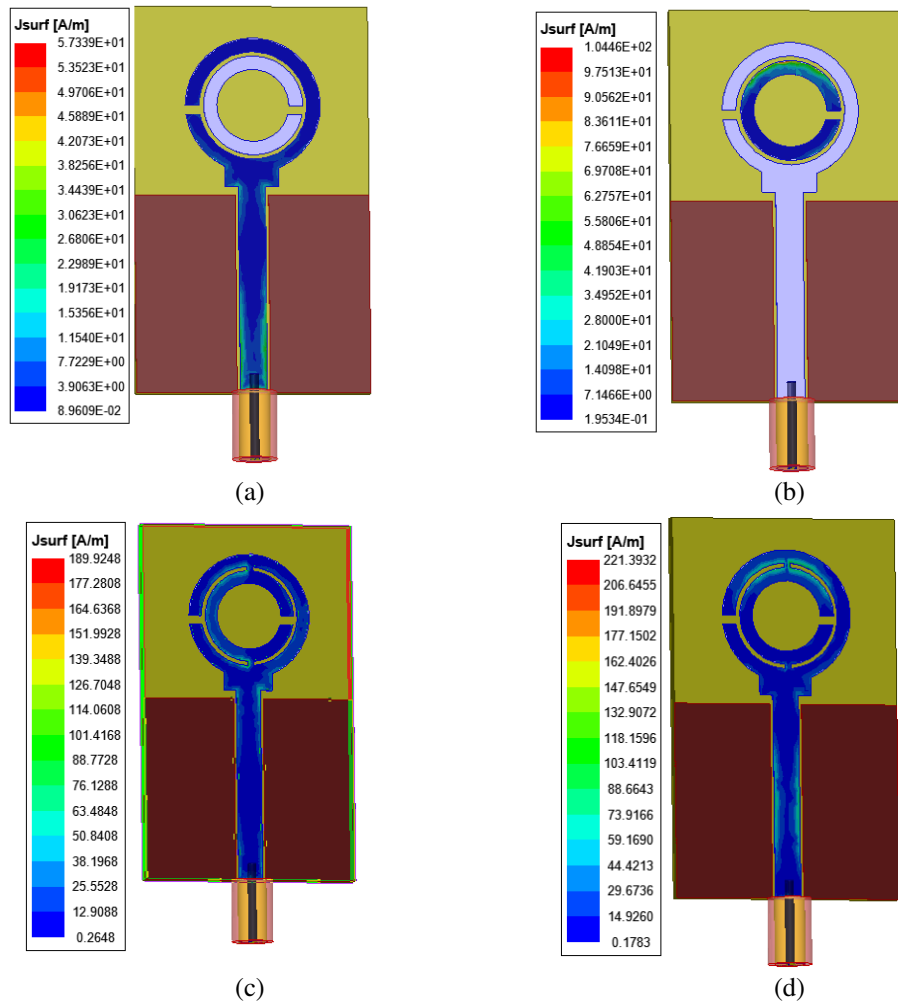


**Figure 10.** Surface current distribution of the C-SRR antenna without metallic loading (a) at 2.4 GHz, (b) at 5.2 GHz and C-SRR antenna with metallic loading (c) at 2.4 GHz, (d) at 5.2 GHz.

With the impact of metallic loading, the surface current density is uniformly distributed, and thus higher radiation area leads to wide bandwidth as shown in Figures 10(c)–(d), where it is 12.9 to 38.20 A/m at 2.4 GHz, and at 5.2 GHz, it is in the range of 14.93 to 44.42 A/m over both the rings. Hence, in the C-SRR antenna with metallic loading, the current passes through both the rings as they are connected with metallic loadings. In comparison to the previous works [14–16], the discussed antennas have a better impedance bandwidth due to the uniform current distribution [17].

## 5. CONCLUSION

Two structures of SRR based antennas are designed for WLAN (2.4/5.2 GHz) applications as per the IEEE 802.11 a/b standards. The rings of these antennas are modeled as a series-connected parallel resonance ( $L$ ,  $C$ , and  $G$ ) circuit, and a metallic loading between these rings is modeled as a series combination of G-L (conductance-inductance). The numerical values of these elements are obtained from the simulated  $S_{11}$  response for R-SRR and C-SRR antennas, with and without metallic loading at the resonant frequencies. Using this modeling, the impact of metallic loading between SRR rings is studied and verified with measured results of the C-SRR antenna. Hence, the proposed method is suitable for broadband matching applications without using analytical model expressions. The AR values were found higher than 15 dB and confirmed that the proposed antenna is linearly polarised. Based on these properties, such antennas can be employed for various WLAN/5G applications with wide impedance bandwidth characteristics.

## ACKNOWLEDGMENT

The authors would like to thank the Faculty Research Programme (FRP) of the Institute of Eminence (IoE) scheme of the University of Delhi (Letter ref. No. IoE/FRP/PCMS/2020/27 dated 31.12.2020). Authors would like to thank Atma Ram Sanatan Dharma College, University of Delhi and Department of Electronic Science, University of Delhi South Campus for necessary support.

## REFERENCES

1. Pendry, J. B., A. J. Holden, D. J. Robbins, and W. J. Stewart, "Magnetism from conductors and enhanced nonlinear phenomena," *IEEE Trans. Microwave Theory Techn.*, Vol. 47, No. 11, 2075–2084, 1999.
2. Smith, D. R., D. C. Vier, Th. Koschny, and C. M. Soukoulis, "Electromagnetic parameter retrieval from inhomogeneous metamaterials," *Phys. Rev. E*, Vol. 71, No. 3, 036617, 2005.
3. Marques, R., F. Mesa, J. Martel, and F. Medina, "Comparative analysis of edge- and broadside-coupled split ring resonators for metamaterial design — Theory and experiments," *IEEE Trans. Antennas Propagat.*, Vol. 51, No. 10, 2572–2581, 2003.
4. Bonache, J., I. Gil, J. Garcia-Garcia, and F. Martin, "Novel microstrip bandpass filters based on complementary split-ring resonators," *IEEE Trans. Microwave Theory Techn.*, Vol. 54, No. 1, 265–271, 2006.
5. Gil, M., J. Bonache, J. Selga, J. Garcia-Garcia, and F. Martin, "High-pass filters implemented by composite right/left handed (CRLH) transmission lines based on complementary split rings resonators (CSRrs)," *PIERS Online*, Vol. 3, No. 3, 251–253, 2007.
6. Martin, F., F. Falcone, J. Bonache, R. Marques, and M. Sorolla, "Miniaturized coplanar waveguide stop band filters based on multiple tuned split-ring resonators," *IEEE Microw. Wireless Compon. Lett.*, Vol. 13, No. 12, 511–513, 2003.
7. Saadoun, M. M. I. and N. Engheta, "A reciprocal phase shifter using novel pseudo-chiral or  $\omega$  medium," *Microw. Opt. Technol. Lett.*, Vol. 5, No. 4, 184–188, 1992.
8. Antoniadou, M. A. and G. V. Eleftheriades, "A broadband series power divider using zero-degree metamaterial phase-shifting lines," *IEEE Microw. Wireless Compon. Lett.*, Vol. 15, No. 11, 808–810, 2005.
9. Ziolkowski, R. W. and A. D. Kipple, "Application of double negative materials to increase the power radiated by electrically small antennas," *IEEE Trans. Antennas Propagat.*, Vol. 51, No. 10, 2626–2640, 2003.
10. Arnedo, I., J. Illescas, M. Flores, T. Lopetegui, M. A. G. Laso, F. Falcone, J. Bonache, J. García-García, F. Martín, J. A. Marcotegui, R. Marqués, and M. Sorolla, "Forward and backward leaky-wave radiation in split-ring-resonator-based metamaterials," *IET Microw. Antennas Propag.*, Vol. 1, No. 1, 65, 2007.

11. Duk Jang, K., J. Hee Kim, D. Hyun Lee, and W. S. Park, "Compact resonant antenna based on composite right/left-handed transmission line with a magneto-dielectric material," *Microw. Opt. Technol. Lett.*, Vol. 51, No. 8, 1994–1997, 2009.
12. Kim, I. K., H. Wang, S. J. Weiss, and V. V. Varadan, "Embedded wideband metaresonator antenna on a high-impedance ground plane for vehicular applications," *IEEE Trans. Veh. Technol.*, Vol. 61, No. 4, 1665–1672, 2012.
13. Yu, Z., S. Mo, and Z. Long, "A novel UWB SRR antenna," *2011 IEEE International Symposium on Antennas and Propagation (APSURSI)*, 1486–1489, 2011.
14. Cumhuri Basaran, S. and Y. E. Erdemli, "A dual-band split-ring monopole antenna for WLAN applications," *Microw. Opt. Technol. Lett.*, Vol. 51, No. 11, 2685–2688, 2009.
15. Cumhuri Basaran, S., "A compact dual-wideband antenna based on complementary split-ring resonator," *Microw. Opt. Technol. Lett.*, Vol. 54, No. 8, 1917–1920, 2012.
16. Basaran, S. C. and K. Sertel, "Dual wideband CPW-fed monopole antenna with split-ring resonators," *Microw. Opt. Technol. Lett.*, Vol. 55, No. 9, 2088–2092, 2013.
17. Sehgal, P. and K. Patel, "Dual-wideband CPW-fed monopole antenna with circular split-ring resonators," *7th International Conference on Signal Processing and Integrated Networks (SPIN)*, 1078–1083, Noida, India, 2020.
18. Saha, C., "On some studies with split ring resonators SRR of different geometrical shapes for metamaterial applications," Ph.D. Thesis, University of Calcutta, India, 2012.
19. Naqui, J., M. Duran-Sindreu, and F. Martin, "Modeling split-ring resonator (SRR) and complementary split-ring resonator (CSRR) loaded transmission lines exhibiting cross-polarization effects," *Antennas Wirel. Propag. Lett.*, Vol. 12, 178–181, 2013.
20. Marwaha, A., "An accurate approach of mathematical modeling of SRR and SR for metamaterials," *JESTR*, Vol. 9, No. 6, 82–86, 2016.
21. Sadiku, M. N. O., *Elements of Electromagnetics*, Oxford University Press, USA, 1995.